Biomass and Bioenergy 217 (2027) 109799

Contents lists available at ScienceDirect

Biomass and Bioenergy

journal homepage: www.elsevier.com/locate/biombioe

Alkaline resistant tunable superaerophobic bio-based chitosan/dialdehyde starch hydrogels

Vojtěch Škopek [a,b,c,*], Ewa Olewnik-Kruszkowska [d,e], Magdalena Gierszewska [d,e], Iztok Dogsa [f], Paulius Pobedinskas [g,h], Filipa A. Vicente [a,c], Blaž Likozar [a,b], Ilja Gasan Osojnik Črnivec [b,c,**]

[a] Department of Catalysis and Chemical Reaction Engineering, National Institute of Chemistry, Ljubljana, SI-1001, Slovenia
[b] Laboratory for Demonstration of H_2 and CO_2 Technologies, National Institute of Chemistry, Kisovec, SI-1412, Slovenia
[c] University of Ljubljana, Faculty of Chemistry and Chemical Technology, Ljubljana, SI-1000, Slovenia
[d] Department of Physical Chemistry and Physicochemistry of Polymers, Faculty of Chemistry, Nicolaus Copernicus University in Toruń, Toruń, 87-100, Poland
[e] Nicolaus Copernicus University in Toruń, Institute of Advanced Studies, Toruń, 87-100, Poland
[f] University of Ljubljana, Biotechnical Faculty, Department of Microbiology, Ljubljana, SI-1000, Slovenia
[g] Institute for Materials Research (IUMAT), Hasselt University, Hasselt, B-3500, Belgium
[h] IUMAT, IMEC vzw, Wetenschapspark 1, Diepenbeek, 3590, Belgium

ARTICLE INFO

Keywords:
Aerophobicity
Chitosan
Dialdehyde starch
Hydrogel
Swelling
Viscoelasticity
Electrode performance

ABSTRACT

Development of bio-based materials with advanced properties is required to replace synthetic and per- and polyfluoroalkyl-based ingredients, particularly for applications involving solid-liquid-gas interfaces. To enable alkaline-resistant materials with tunable aerophobicity, bio-based chitosan/dialdehyde starch hydrogels were prepared through covalent Schiff base crosslinking. Chitosan molecular weight (250-1800 kDa) and concentration (1.5-4.0% w/v) were varied at fixed crosslinker content (1.0% w/v) to investigate the effect on network formation, viscoelasticity and functionality. Rheological analysis shows that systems with low chitosan content require long gelation times (>30 min) to form viscous materials with storage moduli of 1 Pa and internal porous structure (10-100 μm). In contrast, highly concentrated chitosan gels formed rapidly (<4 min) reaching up to 150 Pa, indicating improved structural strength. Swelling experiments on freeze-dried hydrogels at pH 6.8, 10, and 12 showed water absorption with swelling ratios ranging from 5000 to 1300%, depending on composition. Most systems maintained structural stability over the 7-day swelling test, undergoing limited degradation in alkaline conditions (pH 12). Aerophobicity was evaluated by measuring contact angles of bubbles on submersed (in water or pH 12) hydrogels, which range from 130 to 170°, increasing with both chitosan concentration and molecular weight. The material features were demonstrated for electrode development, improving performance at higher overpotentials (−0.67 V) and increasing alkaline water-splitting efficiency by 15%. The prepared materials thus provide alkaline resistance and tunable properties offering potential for various applications, including gas-evolving electrode coatings, alkaline electrolyzer membranes, anti-corrosion coatings, pollutant absorption, environmental remediation, and sensing technologies.

1. Introduction

Circular bioeconomy has given rise to a paradigm shift in materials science, prioritizing sustainable and resilient development of advanced high-performance functional materials [1,2]. As three-dimensional crosslinked macromolecular networks with exceptional capacity for absorbing water, hydrogels provide a versatile platform for addressing modern technological challenges [3,4]. Development of bio-based materials with advanced properties is required to replace synthetic and per- and polyfluoroalkyl substances (PFAS). The replacement of PFAS is driven by severe environmental and health concerns regarding their persistence and bioaccumulation. Hydrogels offer a compelling

This article is part of a special issue entitled: Biomass Europe published in Biomass and Bioenergy.

* Corresponding author. Department of Catalysis and Chemical Reaction Engineering, National Institute of Chemistry, SI-1001, Ljubljana, Slovenia.
** Corresponding author. Laboratory for Demonstration of H_2 and CO_2 Technologies, National Institute of Chemistry, SI-1412, Kisovec, Slovenia.
E-mail addresses: vojtech.skopek@ki.si (V. Škopek), gasan.osojnik@ki.si (I.G. Osojnik Črnivec).

https://doi.org/10.1016/j.biombioe.2026.109799
Received 29 April 2026; Received in revised form 2 July 2026; Accepted 5 July 2026
Available online 14 July 2026
0961-9534/© 2026 The Authors. Published by Elsevier Ltd. This is an open access article under the CC BY license (http://creativecommons.org/licenses/by/4.0/).

alternative because their highly hydrophilic, water-retaining macromolecular structures can establish stable, biomimetic gas-repellent interfaces without relying on fluorinated synthetic components. The simultaneous possession of elastic characteristics like solid bodies and the penetrability of liquids has allowed the precisely controlled modification of the physicochemical and mechanical properties [2,5]. Hydrogel research is thus rapidly progressing toward advanced materials applications, including energy storage, electrocatalysis, smart sensing, and industrial protection [3,4,6]. However, a major limitation for industrial deployment of hydrogels for advanced applications remains in their insufficient stability under harsh conditions, such as extreme pH, high salinity, and chemically aggressive environments, where conventional hydrogel systems often fail [7–9]. Development of sustainable materials for operation in alkaline conditions is proving to be particularly challenging, while highly relevant for alkaline batteries [10–12], supercapacitors [13], and gas-evolving electrochemical processes [14–18], where pH values frequently exceed 12. Herein, the versatility of hydrogel preparation approaches, ranging from cross-linking based on weak chemical interactions to strong covalent bonding, offers strategies that can be examined to prepare chemically robust hydrogels. Amongst renewable building blocks, chitosan is the only naturally occurring alkaline cationic polysaccharide-stands out due to its reactive amino and hydroxyl functionalities, enabling versatile chemical modification [1,9,19]. Despite its biodegradability and film-forming ability, characteristic to many other polysaccharides and biopolymers, chitosan-based systems also suffer from a particularly critical limitation: instability in alkaline environments [20–22]. I.e., under alkaline conditions, the low chemical and mechanical stability of chitosan typically results in reduced structural integrity or limited chemical features and responsiveness [23]. To overcome these limitations through sustainable approaches, dialdehyde starch (DAS) can offer solutions as an effective bio-based crosslinker [24–26]. Via formation of covalent Schiff base (imine) bonds to the amino groups on the chitosan backbone, a chemical stable chitosan network can be established [27–29]. These bonds form mechanically strong networks in comparison to their physically crosslinked counterparts. Despite these advantages, there is an inadequate understanding of the relationship between the structure-property characteristics formulation, including concentration, polymer chain length, morphology, viscoelastic behavior, and their joint influence on stable long-term operation under extreme conditions. Furthermore, the stability of hydrogel stability is rarely assessed in alkaline conditions during hydrogel development.

Hydrogels development offers solutions in numerous fields. For energy systems, hydrogel-based materials have demonstrated a promising substitute for liquid electrolytes in flexible batteries and supercapacitors which exhibit good ionic conductivity and safety [1,19]. For electrocatalytic applications, such as water electrolysis, bio-based hydrogels are being developed to replace synthetic and PFAS based materials, being particularly promising for gas-evolving systems (porous 3D structured electrodes for alkaline oxygen and hydrogen evolution reactions) and for selective gas-permeation (alkaline anion exchange membranes (AEM) preventing H_2 and O_2 crossover). Herein, efficient control on the solid-liquid-gas interface is important due to limited water supply to the surface of the electrode, that can be caused by the accumulation of bubbles [14,30,31]. Aerophobic or even superaerophobic materials are therefore desirable to facilitate the rate of bubble removal thus potentially increasing the overall system performance. Additionally, hydrogel coatings show strong potential in corrosion protection and antifouling applications by forming hydrated interfaces that limit ion penetration and biological adhesion [3,32–35].

Table 1 presents an overview of current hydrogel applications and their associated challenges. At the same time, it highlights that, despite emerging studies, the research for entirely bio-based hydrogels combining alkaline stability and the controllable aerophobic properties has remained limited. Recent studies [14–18,41,42] have demonstrated that superaerophobic materials for gas-evolving systems are generally based on synthetic components, such as polyallylamine or polyethyleneimine with glutaraldehyde. In contrast, chitosan/DAS hydrogel system investigated in this study provides a bio-based alternative that combines alkaline stability with superaerophobic behavior.

In chitosan-based hydrogels research, several common challenges remain to be addressed: the trade-off between mechanical properties and ion conductivity, long-term stability under cyclic hydration, and stability under highly corrosive chemical environment [22,43–45]. In particular, chitosan hydrogels crosslinked with DAS have attracted increasing attention due to the formation of dynamic Schiff base linkages, providing a fully bio-based route to enhanced structural integrity. However, the lack of systematic studies correlating chemical composition with control of the thickness of the deposition and/or three-dimensional morphology, rheological behavior, and long-term stability in highly alkaline conditions represents a key knowledge gap limiting further research and application.

In this context, the present work focuses on the preparation of bio-based chitosan/DAS hydrogels and their thorough characterization to better understand the link between composition and structure-property relationship, especially focusing on alkaline stability, viscoelastic behavior and superaerophobicity. In particular, selected formulations exhibited tunable aerophobic characteristics and robust structural stability under strong alkaline conditions (pH 12), highlighting their potential as sustainable gels that might be platformed for energy storage

Table 1
Comparative Overview of development and challenges of functional hydrogels for advanced applications.

Hydrogel system	Intended application	Functional feature	Demonstrated effects	Research gap and challenge	Source
Poly (vinyl alcohol) (PVA)/Starch/Carbon nanotubes	Solar water purification	High light-to-heat conversion	95% purification efficiency	Salting-out and path blockage	[36]
PVA/Glutaraldehyde	Alkaline water electrolysis membrane	Suppress gas crossover	Hydrogen crossover values of 0.69% at 10 mA cm^{-2}	Restricted OH^- conductivity	[37]
Tannic acid/Cellulose nanofiber/ Polyacrylamide	Epidermal sensors	Mussel-inspired adhesion	22.5 mS cm^{-1} ionic conductivity at −40 °C; 748% stretchability	Functional decline in harsh air	[38]
Benzotriazole/Poly (hydroxypropyl acrylate – vinyl-triethoxysilane – acetic acid)/ Polyethyleneimine	Anti-corrosion coating	pH-triggered inhibitor release	87% reduction in corrosion current after 24 h; stable for 240 h in neutral/acid salt spray tests	Inorganic/organic compatibility	[34]
Hydrogel/Fe-based amorphous coating	Marine protective coating	Anticorrosion and antifouling	99.8% and 100% resistant to algae and, mussels attachment	Weak adhesion to rigid substrates	[39]
Gelatin/Graphitized carbon nitride	Oil-water separation	Photocatalytic self-cleaning	99% oil-water separation efficiency	High cost and slow reaction	[40]
Graphene-based	Supercapacitor electrode	High specific surface area	193.8 F g^{-1} specific capacitance at 1 A g^{-1}; energy density of 66.8 W h kg^{-1}	Strong restacking of sheets	[13]
Polyallylamine or Polyethyleneimine/ Glutaraldehyde	H_2 production	Scalability, Superaerophobic behavior	Superaerophobic surface (154.6°); decreased diameter of detaching bubble by 31.5%	Synthetic material	[14, 18]

devices, protective coatings and absorbents, and sensor applications in harsh environments.

2. Material and methods

2.1. Chemicals and reagents

All chemicals were used as received without further purification: acetic acid glacial (≥99.7%, Sigma-Aldrich), acetone (≥99.5%, PREG Chemicals), chitosan of varying molecular weight (MW): low (with average MW 250 kDa, 10-100 Cps for 1% solution in 1% acetic acid at 20 °C), medium (with average MW 1250 kDa, 300-1000 Cps for 1% solution in 1% acetic acid at 20 °C), high (with average MW 1500 kDa, 1000-2000 Cps for 1% solution in 1% acetic acid at 20 °C), and very high (with average MW 1800 kDa, 2000-3500 Cps for 1% solution in 1% acetic acid at 20 °C) (Glentham Life Sciences), glutaraldehyde solution (25 wt%) (Sigma-Aldrich), hydrochloric acid (0.25 M) (Reagecon), phenolphthalein (Merck), sodium hydroxide (≥98%, Sigma-Aldrich), sodium periodate (≥99.8%, Honeywell), and soluble starch (from potato, 2 g soluble in 100 ml boiling water, Sigma-Aldrich).

2.2. Degree of deacetylation

The degree of deacetylation (DDA) of chitosan was determined by potentiometric titration, following the Broussignac method [46]. Chitosan solutions (0.2% w/v in 0.02 M HCl) were titrated with a standardized solution of 0.1 M NaOH. Changes in the solution's pH after the addition of a specified volume of titrant were recorded using an ESAgP-309W combined electrode (EUROSENSOR) connected to micro-titrator (model, Cerko Lab System).

Two titration endpoints, corresponding to the volumes of titrant V_1 and V_2 defined below, were identified from the pH = f(V) plot using the first derivative method. For this purpose, plots of ΔpH/ΔV = f(V) were prepared, where ΔpH and ΔV denote the increments between successive changes in pH and titrant volume, respectively. The DDA was calculated as shown in Eq. (1).

$$DDA\ [\%] = \frac{M_{GlcNAc} \cdot C_{NaOH} \cdot (V_2 - V_1)}{m_{Ch} + C_{NaOH} \cdot (M_{GlcAc} - M_{GlcN}) \cdot (V_2 - V_1)} \cdot 100\% \quad (1)$$

Where C_{NaOH} is the molar concentration of the titrant (mol/L), m_{Ch} is the chitosan sample mass (g), V_1 is the titrant volume to neutralize HCl (L), V_2 is the titrant volume to neutralize HCl and protonated amino groups (L), M_{GlcAc} is the molar mass of 2-acetamido-2-deoxy-D-glucopyranose (g/mol), and M_{GlcN} is the molar mass of 2-amino-2-deoxy-D-glucopyranose (g/mol).

2.3. Dialdehyde starch preparation

DAS crosslinker was prepared by selective oxidation with sodium periodate ($NaIO_4$) by modifying the procedure described by Ziegler-Borowska et al. [47]. In brief, a suspension was prepared by mixing 3 g of starch in 80 mL of distilled water. Additionally, a solution of sodium periodate was prepared by dissolving 3 g (0.165 M) in 85 mL of distilled water; to fully dissolve it, a sonication bath was used for 30 min. The starch suspension was magnetically stirred (450 rpm) in a round-bottom flask and placed in a water bath at 40 °C; the sodium periodate solution was added from an addition funnel over 25 min. The reaction lasted 3 h from the start of the oxidant addition. The reaction mixture and the addition funnel were covered with aluminum foil to prevent any $NaIO_4$ degradation. After the reaction was finished, the mixture was cooled in air for 15 min and then DAS was precipitated with 250 mL of cold acetone. The precipitated product was filtered using a glass filter and washed three times with distilled water (250 mL), acetone:water (1:1, 120 mL), and finally with acetone (80 mL). The product was dried in a vacuum oven overnight (18 h) at 25 °C and homogenized using a mortar. The formation of new aldehyde groups was confirmed by Fourier transform infrared (FTIR) spectroscopy, and the dialdehyde content was determined by alkaline titration.

2.4. FTIR spectroscopy

The formation of new aldehyde groups was confirmed by FTIR spectroscopy. FTIR spectra were recorded at room temperature (25 °C) from 4000 to 400 cm^{-1} with the resolution of 4 cm^{-1} for 32-scans/sample with an inserted diamond ATR-FTIR device (Spectrum Two, PerkinElmer).

2.5. Determination of aldehydic content

The aldehydic content was determined via alkaline titration according to the modified procedure of Zuo et al. [25]. Firstly, 0.1 g of DAS was dissolved in 5 mL of NaOH solution (0.25 mol/L). The mixture was completely dissolved in a sonication bath for 5 min. When the prepared solution changed color from transparent to orange, 7.5 mL of HCl (0.25 mol/L) was added and shaken, producing; a color change to pale yellow. Activated charcoal was added and the mixture was shaken for 2 min and the solution was filtered using a polytetrafluoroethylene (PTFE) syringe filter (0.45 μm), to obtain a colorless and transparent solution. To perform the titration, three drops of phenolphthalein were added and the solution was then, titrated with NaOH solution (0.25 M). A persistent color change of the solution to purple (color did not fade within 30 s) indicated the titration end point. Measurements were repeated 3 times. The following Eq. (2) was used to determine the number of converted glucose units within the starch sample:

$$ALD\ [\%] = \frac{C_1 \cdot V_1 + C_2 \cdot V_2 - C_3 \cdot V_3}{\frac{m}{161} \cdot 1000} \cdot 100\% \quad (2)$$

where C_1 (mol/L) is the concentration of NaOH solution, V_1 (mL) is the volume of NaOH solution, C_2 (mol/L) is the concentration of NaOH solution used for titration, V_2 (mL) is the volume of NaOH solution used for titration, C_3 (mol/L) is the concentration of HCl solution, V_3 (mL) is the volume of HCl solution, m (g) is the mass of DAS, and 161 is the average relative MW of the repeating unit of DAS.

Several alternative FTIR methods for DDA determination, utilizing absorbance signals at 1550, 1655, 2870, 2878, or 3450 cm^{-1} are proposed in the literature [48–51], In our study, the absorbance peaks at 1320 and 1420 cm^{-1} were used, as this region is assumed to be least affected by signal overlapping and by potential moisture interference [52].

Absorbance values were used to calculate the degree of acetylation (DA) and, subsequently, the DDA according to Eq. (3) as described by J. Brugnerotto et al. [53]:

$$DA[\%] = \left(\frac{A_{1320}}{A_{1420}} - 0,3822\right) \Big/ 0,03133\ DDA[\%] = 100 - DA \quad (3)$$

2.6. Hydrogel synthesis

Chitosan was completely dissolved in 2% (v/v) acetic acid solution under magnetic stirring (250 rpm, overnight) at room temperature (25 °C) to obtain 1.5, 2, 2.5, 3, 3.5, and 4% (w/v) chitosan solutions. DAS was dissolved in distilled water, mixed in a heating bath at 95 °C for 15 min, and cooled afterwards to obtain 1% (w/v) DAS solution. Hydrogels were prepared by mixing chitosan and DAS solutions in a 1:1 (w/v) ratio at room temperature (25 °C), immediately starting Schiff base formation. Hydrogels were cured overnight (18 h) to allow completion of the crosslinking.

As reference crosslinker, glutaraldehyde (0.4% w/v) was also for a comparison of gelation extent and properties. These hydrogels were prepared by mixing chitosan and glutaraldehyde solution in a 1:1 (w/v)

ration at room temperature (25 °C).

2.7. Swelling/stability measurements

Prior to the swelling test, hydrogel samples were freeze-dried (for 48 h at 50 °C and a pressure of 0.12 mbar) to remove traces of water and individually weighed. The dry matrices were submerged at 25 °C in 20 mL of different solutions of NaOH (pH 10 and 12) and distilled water (pH 6.8). The swollen samples were drained and weighed at specific time, namely after 15 min, 30 min, 45 min, 60 min, 2 h, 3 h, 4 h, 5 h, 6 h, 1 day, 2 days, 3 days, 4 days and 7 days. All samples were studied in triplicates. To describe swelling behavior following Eq. (4) was used:

$$swelling\ ratio\ [\%] = \frac{m_2 - m_1}{m_1} \cdot 100\% \quad (4)$$

where m_1 is the mass of the sample before swelling and m_2 is the mass of the sample after swelling at a certain time.

2.8. Rheological measurements

To determine gelation times and viscoelastic behavior, MCR 302 rheometer equipped with a parallel-plate geometry (PP25, d = 25 mm), P-PTD 200 temperature control system and Rhecompass software (v. 1.35) (all Anton Paar) were used. Measurements were carried out with a set gap of 1.5 mm, at 20 °C1% constant shear strain, 1 Hz frequency and normal force set to constant 0 N. Time sweep measurements were carried out for at least 30 min after mixing the crosslinking agent (1% w/v DAS or 0.4% w/v glutaraldehyde) with the polymer solution. The total time required for hydrogel preparation was 4 min, including 1 min of mixing, pouring the solution onto the rheometer plate, and trimming of the excess sample. Storage modulus (G′), loss modulus (G″), loss factor (tan δ), complex viscosity (η*), torque, and normal force were recorded as a function of time. Gelation time was defined as the crossover point of G′ and G, corresponding to tan δ = 1.

2.9. Scanning electron microscopy (SEM)

Hydrogel samples were freeze-dried before analysis and sputter-coating before analysis was not needed. Imaging of aerogels was obtained by scanning electron microscope HR-SEM, Zeiss Supra 35 VP. The analysis was performed with aperture size 30 μm in high vacuum with low accelerating voltage (EHT) of 1 kV (magnification 100-800x, working distance 4.0-6.7 mm) to prevent any sample destruction.

In order to roughly preserve the structural features of the hydrated network, prevent pore collapse and minimize artefacts associated with ice-crystal formation, a flash-freezing step with liquid nitrogen was applied before freeze-drying.

To examine internal morphologies, aerogels were cut to expose cross-sections. Due to their flexible and sponge-like nature, samples were frozen in liquid nitrogen to increase brittleness and enable clean fracture for observation. Frozen materials were then cut into multiple orientations to account for the random pore distribution. Thin sections were mounted onto carbon tape and gently fixed using compressed air to ensure proper adhesion. SEM imaging was performed without conductive coating to avoid potential alterations in morphology. Instead, a low vacuum and low accelerating voltage (1 kV) was used to minimize beam-induced damage and charging effects.

2.10. Contact angle measurements

A contact angle analysis system (OCA 15plus, DataPhysics) was used to determine aerophobic properties of hydrogel samples with the captive bubble method. After mixing the chitosan polymer with the crosslinking agent, the mixture was immediately poured onto nickel plates (10mm × 10 mm) and spread evenly to fully cover the surface. Hydrogels were cured at ambient temperature (25 °C) in the dark overnight (18 h) by freely evaporating solvents. After curing, the hydrogel coated plates were rehydrated in either distilled water (pH 5.5) or KOH solutions (pH 12) for 10 min and placed in cuvettes filled with either distilled water or KOH solutions (pH 12). A needle with manual air control released a bubble of 8 μL. Once the bubble settled on the surface, the recording started. Bubble drop measurements were conducted in triplicate at ambient temperature (25 °C), each time on a slightly different location on the coated plate. The final contact angle value was calculated as the average of contact angles on both sides of the captured image of the bubble.

2.11. Coating of electrode and electrochemical characterization

Hydrogel coatings were deposited on platinum plates (10 × 10 mm) with a spin-coater (WS-400-6NPP-Lite, Laurell). Two coatings examined by depositing 100 μL of 3% (w/v) chitosan solution with either low or very high MW chitosan. Chitosan solutions were dispensed onto platinum plates immediately prior to spinning, followed by spin-coating at 8000 rpm for 40 s.

During the last 10 s of the spin-coating, 100 μL of 1% (w/v) DAS crosslinking solution was applied onto the rotating substrate. The coated electrodes were then kept in the dark overnight to allow complete curing of the hydrogel layer.

Electrochemical measurements were carried out with a CHI660E workstation (CH Instruments) at room temperature (25 °C). A three-electrode configuration was used, consisting of the coated platinum plate as the working electrode (cathode), a Hg/HgO (1 M KOH) reference electrode, and a Pt/Ti mesh (25 × 25 mm) as the counter electrode. All measurements were performed in 1.0 M KOH electrolyte at pH 14.

All potentials are relative to the reversible hydrogen electrode (RHE) scale Eq. (5):

$$Voltage\ (V\ vs.\ RHE) = Voltage\ (V\ vs.\ Hg/HgO) + 0.098 + 0.0591 \quad (5)$$

Prior to measurements, the electrodes were immersed in the electrolyte for at least 15 min to allow sufficient swelling of the hydrogel. Linear sweep voltammetry (LSV) was conducted at a scan rate of 10 mV s^{-1}. LSV measurements evaluate electrochemical performance by recording current as a function of applied potential, revealing performance changes, particularly at higher overpotentials associated with rapid hydrogen evolution.

3. Results and discussion

3.1. Characterization of chitosan

DDA of chitosan represents a key parameter for understanding the charge density, reactivity, and chemical structure. In this study, two independent analytical methods were employed to determine the DDA and, consequently, the content of free amino groups in the individual chitosan batches.

For the FTIR spectroscopy analysis of DDA, the collected spectra were subjected to baseline correction, followed by manually defining a baseline and then extracting absorbance values at 1320 cm^{-1} and 1420 cm^{-1} (see Fig. 1).

Across all chitosan batches (including low-, medium-, high-, and very high- MW), relatively comparable DDA values were obtained (Table 2). Nevertheless, FTIR-based determination of acetylated and deacetylated units in chitosan is generally regarded as semi-quantitative. Therefore, the obtained values were considered only as preliminary estimations (Table S1 in Supplementary materials).

According to the study by R. Czechowska-Biskup et al. [52], potentiometric titration represents the most reliable non-NMR technique for quantitative determination of DDA. Thus, further DDA characterization was performed also using the Broussignac potentiometric titration method [46], intended to quantify the number of free amino groups in

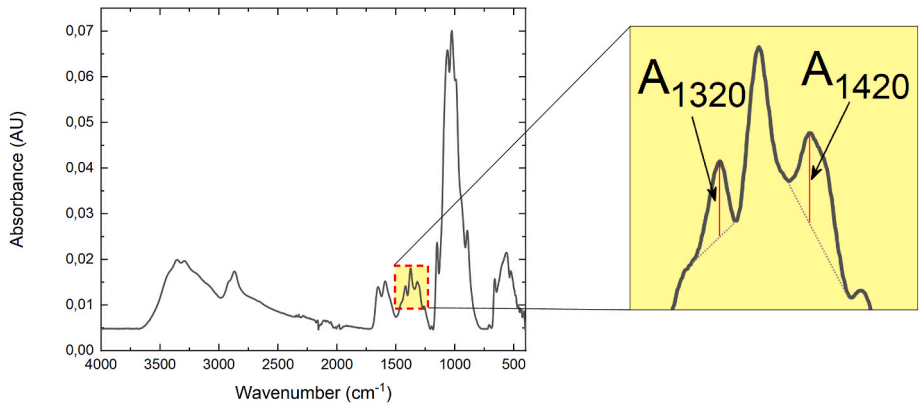


Fig. 1. Example of FTIR spectra of chitosan with highlighted area for absorbance subtraction at wavenumbers 1320 cm^{-1} and 1420 cm^{-1}.

Table 2
Comparison of FTIR and potentiometric method of determining degree of deacetylation of chitosan. Data are means ± SD (n = 3).

	DDA [%] determined by:	
	FTIR	potentiometric titration
Chitosan Low MW	79.2 ± 0.6	85.31 ± 1.0
Chitosan Medium MW	77.8 ± 0.4	86.91 ± 3.1
Chitosan High MW	77.4 ± 0.4	86.51 ± 0.1
Chitosan Very High MW	76.2 ± 0.9	86.06 ± 3.2

chitosan polymer. In this procedure, chitosan is first dissolved in an excess of HCl. The remaining acid is subsequently back-titrated with NaOH while continuously monitoring the pH response. The first equivalence point (V_1) corresponds to the neutralization of excess HCl, whereas the second equivalence point (V_2) represents the deprotonation of all NH_3^+ groups in chitosan chain. Thus, the difference between these two equivalence points corresponds to the exact amount of free amino groups present in the polymer (Tables S2–5 and Fig. S1–4).

Comparing the results of the two different methods revealed differences in DDA values measured by FTIR and potentiometric titration, with deviation of approximately 6-10% (Table 2)and an observed difference in the general trend of DDA versus MW, where chitosan with low MW was determined for higher DDA value by FTIR and lower with potentiometric titration, and vice versa for chitosan with very high MW. While there were no statistically significant differences between measurements, suggesting a good degree of precision, systematic discrepancies in the absolute DDA values were found, indicating poor absolute accuracy. The literature [52] recognizes potentiometric titration as a more accurate and reliable method for the determination of DDA and, hence, we assume that the results obtained by this method are more representative of the true DDA values of our chitosan samples.

Based on these values, chitosan contains a high abundance of free amino groups, which play a crucial role in the crosslinking step, where the aldehyde groups of DAS primarily react with the amino groups of chitosan.

3.2. Preparation of bio-based crosslinker - dialdehyde starch

Due to the presence of accessible primary amino groups within the chitosan structure, dialdehydic material was selected as suitable bio-based crosslinking agent for rapid and effective covalent imine bonding, enabling efficient crosslinking even in the absence of additional catalysts. The dialdehyde polysaccharide was prepared via selective oxidation of vicinal diols using sodium periodate (see mechanism Fig. S5).

Efficient removal of a residual oxidant was a critical step in the preparation procedure. A recent study [29] report washing the final product only with an acetone:water (1:1), however for our purpose, this washing procedure proved insufficient. Namely, after washing deposits of crystalline structures were visible under SEM morphological examination, which SEM-EDX analysis revealed to be the remaining traces of inactive periodate ions (Fig. S6).

The washing procedure was thus improved. The product was sequentially washed with water (250 mL), an acetone:water (1:1) mixture (120 mL), and finally, pure acetone (80 mL). The initial water washing was an essential step for removing ionic residues. Subsequently, the acetone:water mixture was used to ensure a gradual change in solvent polarity, preventing potential structural collapse of the oxidized polysaccharide and minimizing possible side reaction. The final washing step with pure acetone was performed in small subsequent portions to replace the remaining water trapped in the product, thereby increasing the volatility of the remaining solvent and accelerating the subsequent drying process.

Drying was performed overnight (16 h) in a vacuum oven at 25 °C. After complete solvent removal, the prepared dialdehyde starch was homogenized using a mortar. SEM-EDX analyses confirmed complete removal of iodine-containing residues from the oxidant in the final product (Fig. S7).

After the procedure, formation of aldehyde groups on starch was confirmed by FTIR spectroscopy (see Fig. 2). A new absorption band characteristic of carbonyl stretching C=O in aldehydes was observed at approximately 1700 cm^{-1}. Changes in the 3000-3600 cm^{-1} region

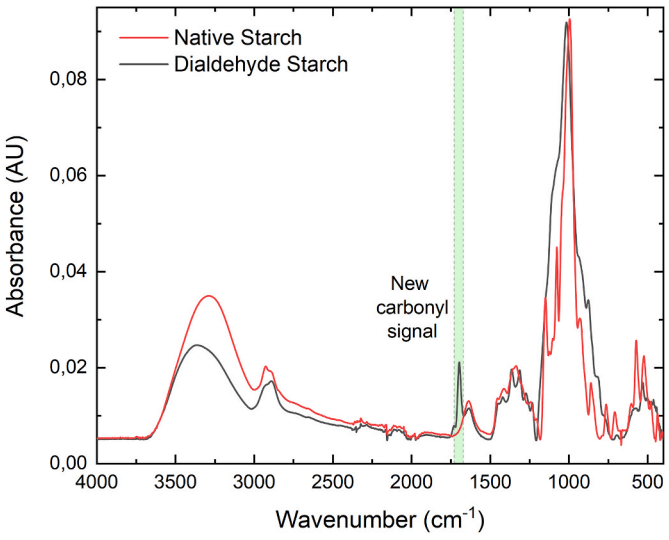


Fig. 2. FTIR spectra of native and modified starch confirming creation of new carbonyl bond.

correspond to O–H stretching vibrations and alterations in hydrogen bonding, indicating transformation of hydroxyl groups. Additionally, the 2800-3000 cm^{-1} region reflects changes in asymmetric C–H stretching vibrations, while the 400-900 cm^{-1} region shows variations associated with C–H and C–OH deformation modes. In contrast, the 900-1200 cm^{-1} region, corresponding to C–O–C stretching vibrations, remained largely unchanged in intensity, indicating that proceeds selectively via cleavage of vicinal diols without significant degradation of the polysaccharide backbone.

Most importantly, aldehyde content was quantified by alkaline titration in order to determine the degree of functionalization of the starch. This parameter is crucial for evaluating the reactivity of the crosslinker in subsequent reactions with the amino groups of chitosan. The aldehyde content of the prepared DAS was determined to be 63.7 ± 1.2%, consistent with values reported in the literature [47].

3.3. Hydrogel synthesis

Starch shows limited solubility in water, even after modification. Therefore, additional heating of the mixture is required for complete dissolution of the DAS for further processing. This was achieved by continuous stirring of the DAS-water suspension in a water bath at 95 °C for 15 min, resulting in a fully dissolved starch solution with a transparent appearance. After cooling to room temperature (25 °C), the solution was filtered using a PTFE syringe filter with pore size 0.45 μm to remove any insoluble residues. The crosslinking agent DAS was prepared for use at a final concentration of 1% (w/v).

Similarly, because chitosan is considered a weak base, it is not soluble in water or most organic solvents. Protonation of the glucosamine units to the soluble R-NH_3^+ form is required. This was achieved by dissolving chitosan in a diluted aqueous acidic solution; in this case, 2% (v/v) acetic acid was used. Fresh chitosan solutions were prepared at various concentrations (1.5-4% (w/v)) by stirring in the acidic environment until fully solubilized overnight at room temperature (25 °C). Higher chitosan concentrations required extended dissolution times.

Once the reagents were prepared, hydrogels began to form immediately upon simple mixing. No additional catalyst or elevated temperature was required, although we were able to increase the reaction rate by increasing the temperature. In this study, a fixed concentration of the crosslinker solution was used, by varying the concentration and MW of the chitosan solutions. This approach allowed us to evaluate the direct influence of chitosan concentration and MW on hydrogel formation. The volume ratio of the mixed crosslinker and chitosan solutions was maintained at 1:1 for all measurements.

In this study, we focused on the utilization of the aldehydic reactive groups of the prepared crosslinker and the free amino groups of the chitosan polymer. Gelation is achieved by addition of primary amine of chitosan to an aldehyde group of DAS forming new covalent bond (Fig. 3). The final products are a Schiff base, specifically an imine compound, and a released molecule of water.

3.4. Rheometric study

Rheological measurements were performed to evaluate gelation kinetics and the development of mechanical properties in chitosan/DAS hydrogels. In contrast to low-molecular-weight crosslinkers, DAS contributes to network formation not only through covalent imine bond formation with chitosan amino groups, but also via physical chain entanglement and secondary intermolecular interactions. This dual contribution is characteristic of polymeric crosslinkers and can significantly influence the final network architecture.

Rheological measurements were conducted to monitor the time-dependent evolution of viscoelastic properties during gelation. Experiments were performed under constant oscillatory conditions. Chitosan solutions with concentrations ranging from 1.5 to 4.0% (w/v) were mixed with DAS at a fixed concentration of 1.0% (w/v). For comparison, glutaraldehyde was employed as a low-molecular-weight crosslinker, with its concentration adjusted (0.4% w/v) to provide an equivalent molar content of aldehyde groups.

All measurements were conducted for at least 30 min following the onset of gelation. To minimize experimental variability, samples were mixed vigorously for 1 min, transferred onto the rheometer, and measured after a fixed delay of 4 min, accounting for rapid gelation in some systems. The results (Fig. 4) indicate faster gelation kinetics at increased chitosan concentrations. Higher polymer concentration exhibits significantly faster gelation, reflecting a higher probability of intermolecular interactions and crosslinking stability. Similarly, increasing MW leads to faster network formation, as longer polymer chains promote enhanced entanglement. However, the relationship between MW, concentration and mechanical properties were not strictly proportional. For example, hydrogels prepared with 3.0% (w/v) high MW (1500 kDa) chitosan exhibited a storage modulus after 30 min (G' = 82 ± 8 Pa) comparable to those prepared with very high MW (1800 kDa) chitosan (G' = 60 ± 15 Pa), despite identical conditions as well as closely matching DDA. This non-linear trend may reflect limitation effects of chain entanglements and chain mobilities at very high MW, which might limit network rearrangement and the formation of additional elastically effective crosslinks.

A comparison with glutaraldehyde-crosslinked systems further demonstrates the effect of crosslinker structure on the system. The hydrogels formed with the glutaraldehyde were generally slower forming with a lower storage modulus (Fig. 5). This confirms that DAS improves gel network formation by not only relying on covalent interactions but additional physical forces as well. However, for 4.0% (w/v) very high MW chitosan glutaraldehyde-crosslinked hydrogels displayed higher storage modulus values compared to system with DAS. This suggests that small-molecule crosslinkers can achieve higher crosslink densities, as their minimal steric hindrance facilitates easier

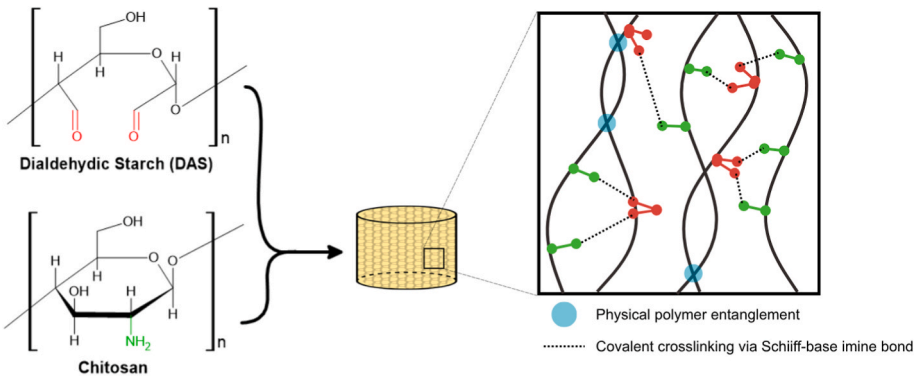


Fig. 3. Visualization of entanglement of DAS and chitosan forming hydrogel. Modified from Aslzad et al. [27].

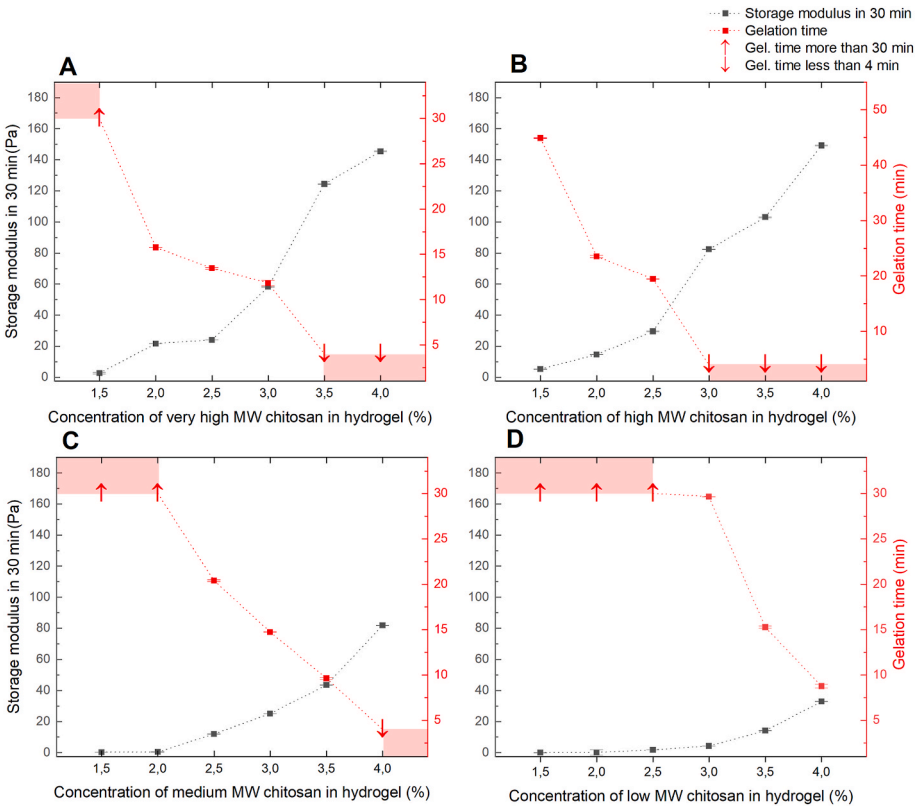


Fig. 4. Viscoelastic properties and gelation kinetics of DAS-crosslinked hydrogels at constant crosslinker concentration 1% (w/v) for chitosans with different MW: (A) very high, (B) high, (C) medium, and (D) low MW. Storage modulus (G′, gray markers) was measured after 30 min, while gelation time (red markers) was determined at the crossover point (tan δ = 1). The red shaded region indicates an estimated gelation window in cases where gelation occurred too rapidly (before 4 min) or too slowly (after 30 min) for precise determination. Data are means ± RSD (n = 3). (For interpretation of the references to color in this figure legend, the reader is referred to the Web version of this article.)

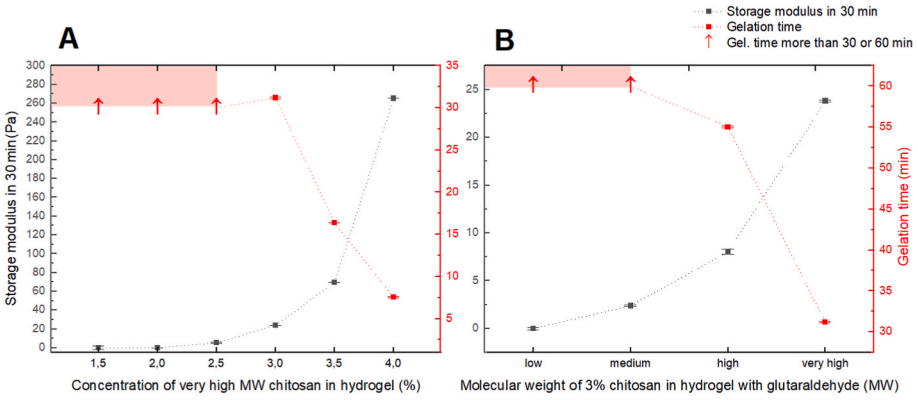


Fig. 5. Influence of (A) very high MW chitosan concentration and (B) chitosan MW on the viscoelastic properties and gelation kinetics of chitosan/glutaraldehyde hydrogels with constant glutaraldehyde concentration 0.4% (w/v). Storage modulus (G′, gray markers) was measured after 30 min, while gelation time (red markers) was determined at the G'/G″ crossover point (tan δ = 1). The red shaded region represents an estimated gelation window in cases where gelation occurred too slowly (after 30 or 60 min) for precise determination. In panel (B), MW varies from low to very high. Data are means ± RSD (n = 3). (For interpretation of the references to color in this figure legend, the reader is referred to the Web version of this article.)

access to reactive sites within the polymer chain. In general, these results indicate that gelation and mechanical properties are influenced by the synergistic effects of polymer concentration, MW and crosslinker structure. Although increased chitosan concentration accelerates gelation and stiffness, MW influence is non-linear, which accounts for both chain entanglement and mobility. Additionally, intermolecular interactions might provide additional structural reinforcement when a polymeric crosslinker is used, such as DAS, highlighting its potential for designing hydrogels with tunable and application-specific mechanical properties.

3.5. Pore size distribution

The morphology of freeze-dried hydrogels (aerogels) and visible porous structures was evaluated and measured under using SEM.

Representative images from multiple regions were analyzed to assess pore size distribution and overall morphology, maintaining relatively well-established unimodal size distribution curves (see Fig. S8–11). The

results (Fig. 6) indicate that variations in chitosan concentration and MW have a limited effect on the average pore size but significantly influence pore architecture.

For the lowest chitosan concentrations, open and highly interconnected networks with large pore sizes were obtained. Due to these large open voids offering insufficient structural support, samples had brittle and uneven morphologies (see Fig. S8), making pore sizes difficult to measure accurately. More compact structures with slightly smaller pore size appeared at higher concentrations.

Across all examined dry samples, pore sizes were predominantly in the range of several tens of micrometers (10-80 μm). To justify these varying trends, two orthogonal directions were measured for each pore, accounting for a potential irregular pore shape. It appears that overall pore interconnectivity and consistency are related strongly to the polymer concentration, whereas absolute pore size is less dependent on it. Interestingly, these morphological features could be further directly linked to aerophobic behavior discussed in Section 3.7, where surface compactness and pore structure influenced bubble adhesion. The relationship between pore structure (size and interconnectivity), the resulting aerophobic and mechanical properties is a critical factor in hydrogel performance. Smaller and more uniformly distributed pores enhance aerophobic behavior by limiting gas bubble adhesion, whereas highly interconnected porous structures provide opposite effect. From a mechanical perspective, reduced pore size generally leads to thicker pore walls and a higher polymer volume fraction, resulting in increased stiffness. In contrast, larger open pores can compromise mechanical integrity due to reduced network density. These observations highlight that tuning pore architecture is essential for optimizing both mechanical and aerophobic performance of chitosan/DAS-based hydrogels.

Similarly, Kang et al. [14] demonstrated that pore sizes in the range of tens of micrometers are optimal for bubble repellency in water-splitting systems while maintaining efficient mass transport. This supports the potential applicability of chitosan/DAS-based hydrogels as functional coatings in such environments.

3.6. Swelling behavior and degradation

The prepared hydrogels were evaluated for their swelling behavior and long-term stability in different aqueous environments (deionized water of pH 5.5, NaOH solutions of pH 10 and 12). Testing conditions were selected to assess their compatibility with alkaline media, *e.g.* as conventional electrolyzers used for electrochemical water splitting typically operate at highly alkaline conditions (up to pH 14). Loss of mass over time does not necessarily mean polymer degradation but also could more likely involve leaching of unreacted or loosely bonded components, especially in an alkaline environment. Swelling measurements provided insight into the time-dependent behavior of the hydrogels and their structural integrity over extended incubation periods. As all chitosan samples exhibited comparable DDA values, the observed differences are primarily attributed to variations in MW and polymer concentration rather than functional group availability. It should be noted, however, that when the chitosan concentration is varied while the DAS content is kept constant, the effective CHO/NH_2 molar ratio also changes and may therefore contribute to the observed behavior (Table S6). Despite the intrinsically dynamic nature of Schiff bases, the hydrogel networks retain their structural integrity and functional performance throughout the investigated period.

For hydrogels prepared with low MW chitosan (Fig. 7) prepared using less concentrated chitosan solutions exhibited the highest swelling ratios (up to 5000%) in all swelling media, owing to their more loosely crosslinked structure and higher free volume, which promotes solvent uptake. However, samples with 1.5% (w/v) chitosan showed a gradual decrease in swelling ratio over time, indicating insufficient crosslinking and structural instability. This behavior is likely associated with the leaching of unbound polymer fractions during prolonged immersion. Interestingly, under strong alkaline conditions (pH 10 and 12), the 1.5% (w/v) low MW chitosan hydrogels exhibited even higher swelling ratios, reaching values up to approximately 5000%, accompanied by a slower swelling decrease. This behavior can be attributed to the pH-responsive

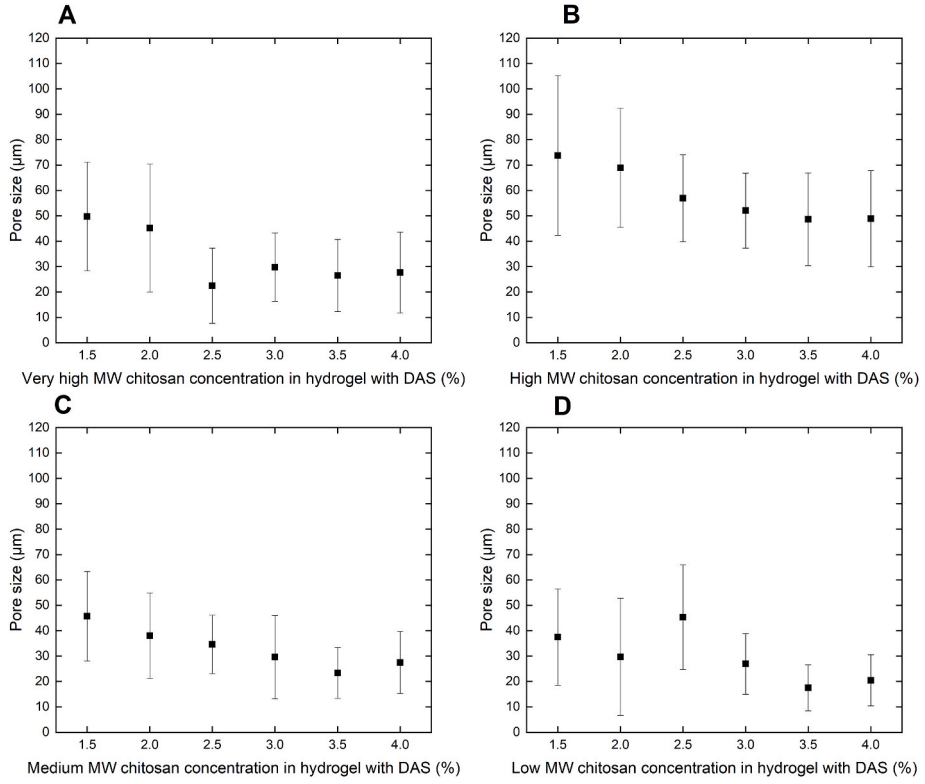


Fig. 6. SEM-derived pore size distribution of chitosan/DAS hydrogels as a function of chitosan concentration for different MWs: (A) very high, (B) high, (C) medium, and (D) low MW chitosan. Data are means ± SD ($n \geq 100$).

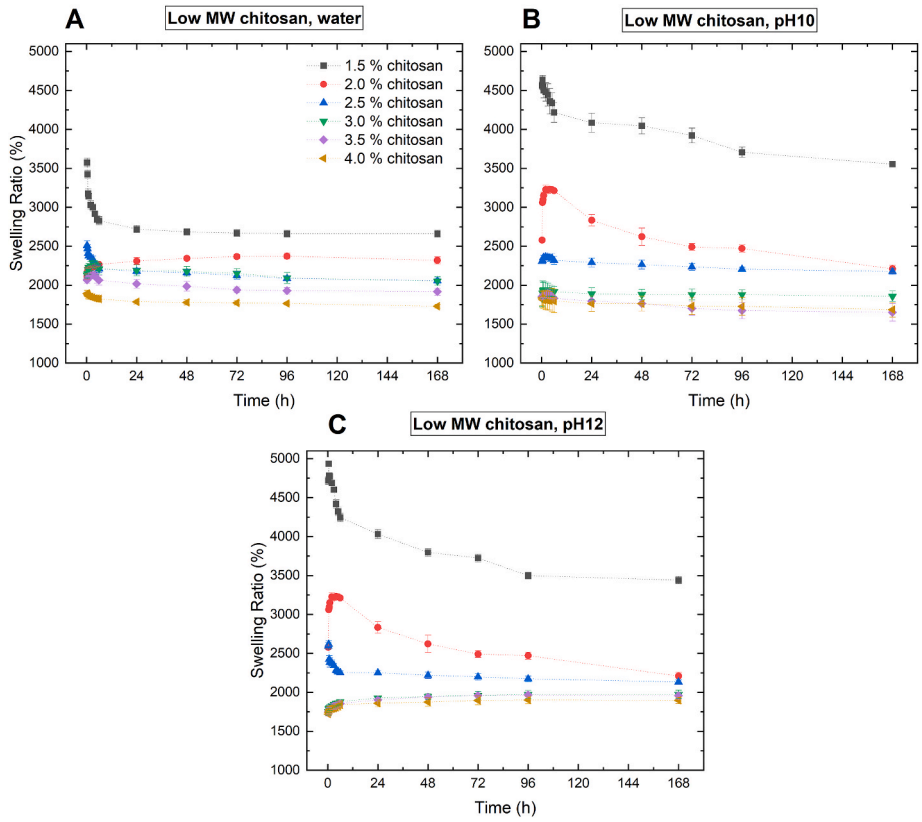


Fig. 7. Time-dependent swelling behavior of hydrogels with varying low MW chitosan concentrations at constant DAS content under different pH conditions: (A) water, (B) pH 10, and (C) pH 12. Chitosan concentrations are: 1.5% (w/v) (gray), 2.0% (w/v) (red), 2.5% (w/v) (blue), 3.0% (w/v) (green), 3.5% (w/v) (purple), and 4.0% (w/v) (yellow). Data are means ± SD (n = 3). (For interpretation of the references to color in this figure legend, the reader is referred to the Web version of this article.)

nature of chitosan. At pH 10 and 12, the amino groups are fully deprotonated (pKa of chitosan is between 6.3 and 6.7), eliminating electrostatic repulsion between polymer chains and rendering chitosan insoluble. In weakly crosslinked systems, structural integrity may therefore be maintained not by a fully developed covalent network, but also by the insolubility of the polymer under alkaline conditions. At the same time, the limited mechanical strength of these networks may allow structural rearrangement and chain relaxation, leading to particularly high swelling values.

These observations are in good agreement with the rheological data. Hydrogels with lower chitosan concentrations result in slow gelation kinetics and weak mechanical strength, suggesting an incomplete network formation. Therefore, in hydrogels with 1.5-2.0% (w/v) chitosan, a combination of insufficient crosslinking and pH dependent polymer charge and solubility influences their swelling behavior.

Medium MW chitosan hydrogels exhibited similar trends (Fig. 8). Notably, the 1.5% (w/v) sample at pH 12 maintained a relatively high and stable swelling ratio (~3200%) over one week, suggesting the formation of a stabilized structure under strongly alkaline conditions. Other concentrations showed stable swelling behavior over time, with minimal long-term variation. Swelling ratios for higher concentrations (3-4% w/v) were typically in the range of 1300-1500% at pH 10 and 1800-1900% at pH 12, indicating a more compact and stable network than was achieved with low MW chitosan.

The swelling of high MW chitosan hydrogel varied according to the medium (Fig. 9). In water, these hydrogels exhibited high swelling ratios (up to ~3100%) and maintained structural stability over one week. At pH 10 and 12, only the lowest concentration of hydrogels (1.5% w/v) resulted in a decreasing swelling ratio over time indicating structural instability. The other concentrations maintained stable hydrogels with swelling ratios ranging between 1300 and 1600% at pH 10 and 1700-1900% at pH 12.

Very high MW chitosan hydrogels exhibited similar trends (Fig. 10) to high MW chitosan. The lowest concentrated hydrogel (1.5% w/v) was relatively stable in water but significantly degraded under alkaline conditions, with swelling decreasing from approximately 2200% to 1700% at pH 12. This behavior indicates a fragmentation of the sample. In contrast, the other concentrations exhibited excellent stability in water with minimal changes in swelling with time. Interestingly, degradation was more pronounced at pH 10 than at pH 12, suggesting that strongly alkaline conditions promote the formation of a more compact structure due to a favorable combination of complete deprotonation and reduced polymer solubility.

In conclusion, the swelling behavior exhibited by hydrogels prepared from chitosan of different MW and at different concentrations appears to be a function of swelling by a delicate interplay between the following factors: polymer concentration, MW, crosslinking efficiency, and the effects of pH on dissociation and charge. The rapid initial mass increase observed within the first 60 min suggests that swelling is initially dominated by capillary forces and rapid pore filling within the freeze-dried structure. Subsequently, the swelling process transitions to a slower, diffusion-controlled regime, where solvent uptake is governed by polymer chain relaxation and network constraints. Lower chitosan concentrations (1.5-2% w/v) exhibited slower equilibration, likely due to lower crosslinking density and higher free volume facilitating solvent diffusion. Comparing hydrogels prepared from chitosan of different MW at pH 12 demonstrates a distinct dependence of swelling behavior on polymer size. Specifically, hydrogels with low MW chitosan showed the highest swelling ratios, whereas an increase in MW leads to a gradual reduction in swelling capacity. High swelling ratios observed for low-concentration samples (1.5% w/v) may also be influenced by the ionic strength of the alkaline medium. The presence of OH^- ions can increase

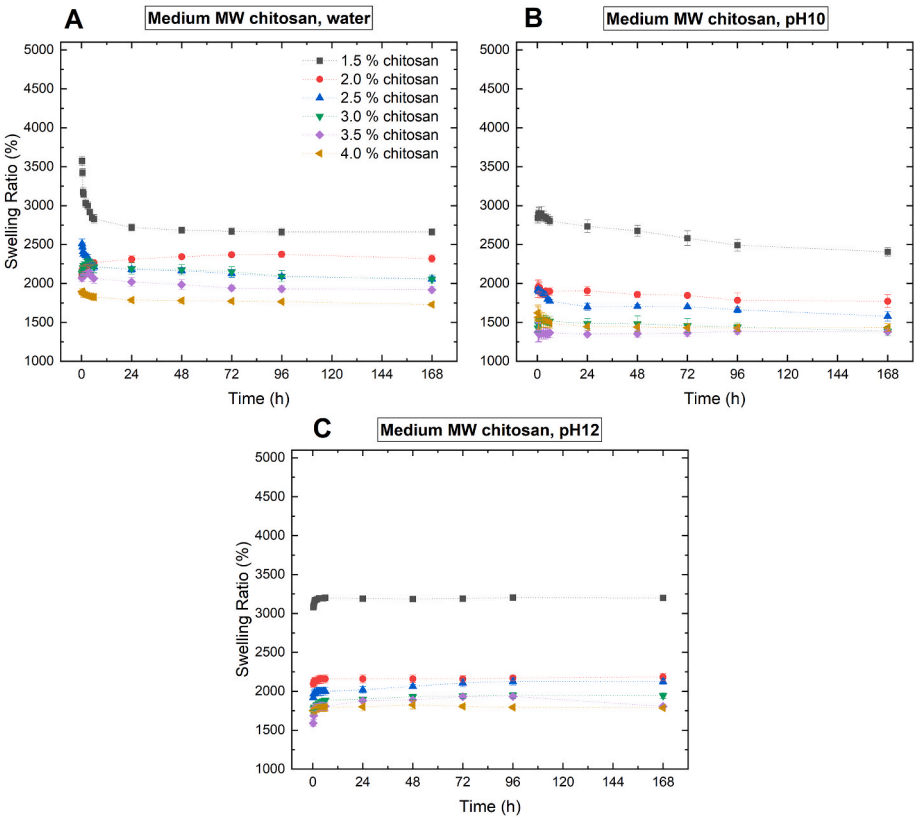


Fig. 8. Time-dependent swelling behavior of hydrogels with varying medium MW chitosan concentrations at constant DAS content under different pH conditions: (A) water, (B) pH 10, and (C) pH 12. Chitosan concentrations are: 1.5% (w/v) (gray), 2.0% (w/v) (red), 2.5% (w/v) (blue), 3.0% (w/v) (green), 3.5% (w/v) (purple), and 4.0% (w/v) (yellow). Data are means ± SD (n = 3). (For interpretation of the references to color in this figure legend, the reader is referred to the Web version of this article.)

osmotic pressure within the hydrogel network, resisting polymer contraction and promoting water uptake. This suggests that, in addition to covalent crosslinking, chain entanglement and ionic effects may contribute significantly to the apparent structural stability under alkaline conditions, which can be expected to be effective particularly at higher MW and polymer concentrations, as already discussed for Fig. 4 in the chapter pretraining to rheometric properties. Increasing the concentration of chitosan leads to a further increase of densification in the polymer network, hence to a reduction of free volume and a limitation of swelling but ensuring a further contribution to gel stability. The polysaccharide backbone of DAS contributes long and flexible crosslinking bridges, permeating a network structure that might improve the mechanical stability at higher concentrations of chitosan.

When the MW of chitosan increases, leaching of hydrogel material is reduced due to both higher MW of chitosan (resulting steric hindrance and subsequent lower diffusivity) and increased crosslinking density. Thus, when low MW chitosan is used, mass reduction over time, especially in loosely crosslinked networks, is more pronounced within the tested period. The differences observed between samples of varying MW are primarily governed by chain length and resulting crosslinking density, as DDA and crosslinker content were consistent across all systems. Under strongly alkaline conditions, deprotonation of amino groups is expected to alter polymer–polymer and polymer–solvent interactions, which may lead to changes in network structure and swelling, such as a decreased ability of water absorption and other structural deformations, thereby affecting final values of swelling ratios.

3.7. Aerophobic properties of hydrogels

Aerophobic properties of the prepared hydrogels were evaluated by measuring the captive air bubble contact angle measurements under water at pH 5.5 and under KOH solution at pH 12. Higher contact angles indicate stronger bubble repellency. This approach enables direct assessment of surface wettability in aqueous environments. Hydrophilicity in chitosan-based systems is governed by the presence of polar functional groups, particularly amino and hydroxyl groups. The DDA plays a key role by determining the density of available amino groups, thereby influencing both water affinity and aerophobic behavior.

The results (Fig. 11) show that increasing both the MW and concentration of chitosan enhances aerophobicity. Higher polymer concentrations increase the density of hydrophilic functional groups, promoting stronger interactions with water and facilitating the formation of a stable hydration layer at the surface. More pronounced differences were observed as a function of MW. Hydrogels prepared from low MW chitosan exhibited slightly reduced aerophobicity (in all cases above 130°), which can be attributed to differences in surface morphology. SEM analysis revealed that low MW and low concentration systems form more porous and less compact surface structures. This morphology might cause air entrapment within irregular surface, limiting effective contact between water and the material and consequently inhibits the ability to repel air bubbles. In strongly alkaline conditions, this effect was even more pronounced, and the hydrogel materials exposed to KOH (pH 12) exhibited enhanced aerophobicity, with lowest values at 145°. This behavior can be attributed to chemical modifications of chitosan under alkaline conditions, including partial deacetylation and possible hydrolysis of glycosidic bonds, which expose additional hydrophilic functional groups on the surface, which confirms the suitability of our chosen base material for use under these conditions. In addition, incompletely crosslinked networks can be expected to result in a higher uniformity and higher relative surface roughness, as well as in the formation of microvoids. These features would appear to disrupt the continuity of the hydration layer, which is essential for

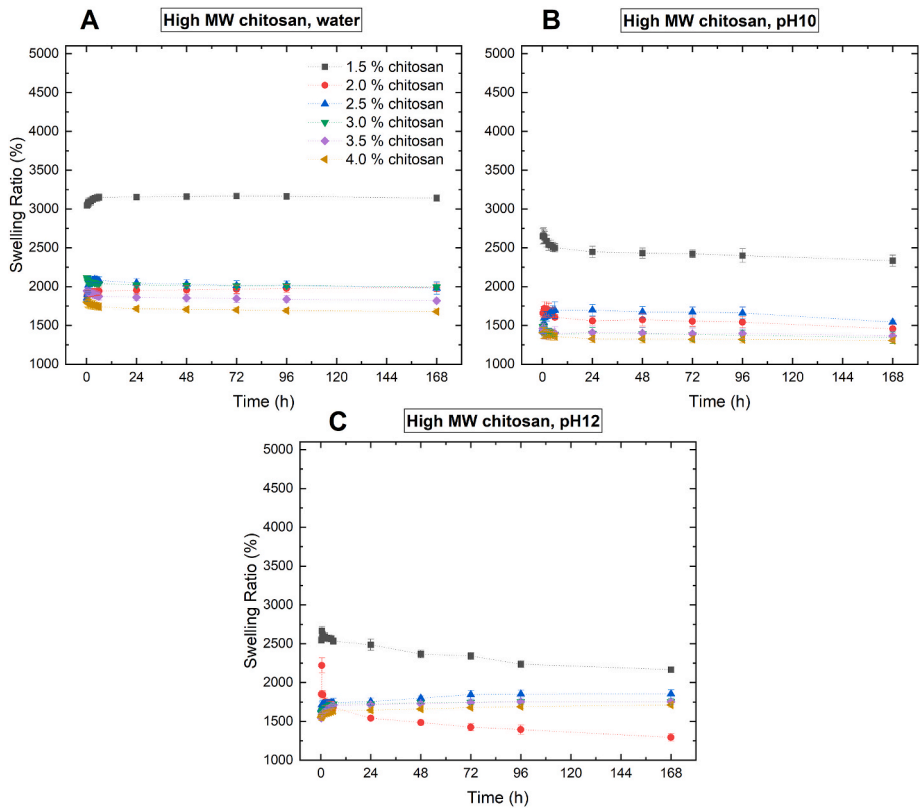


Fig. 9. Time-dependent swelling behavior of hydrogels with varying high MW chitosan concentrations at constant DAS content under different pH conditions: (A) water, (B) pH 10, and (C) pH 12. Chitosan concentrations are: 1.5% (w/v) (gray), 2.0% (w/v) (red), 2.5% (w/v) (blue), 3.0% (w/v) (green), 3.5% (w/v) (purple), and 4.0% (w/v) (yellow). Data are means ± SD (n = 3). (For interpretation of the references to color in this figure legend, the reader is referred to the Web version of this article.)

strong aerophobic behavior. Therefore, aerophobicity is not only dependent on the surface hydrophilicity but also surface morphology, uniformity and mechanical robustness. Rheometric analysis, swelling tests and bubble contact angle measurements therefore jointly suggest that hydrogels with higher MW chitosan and higher polymer concentrations possessed more compact structures, more homogeneous surface morphologies, and denser chain entanglements. These structural improvements appear to minimize air-trapping and optimize surface wetting, leading to enhanced bubble-repellency characterized by exceptionally high contact angles (up to ~170°).

Overall, the experimental results confirm that aerophobic property results from the combined effects of chemical composition and structure. A sufficiently high density of hydrophilic groups on the surface is indeed necessary, however the formation of a well-defined and mechanically robust surface is equally important to achieve sufficient bubble-repellency.

3.8. Coating for enhanced bubble repellency in electrochemical system

To demonstrate the applicability of the developed material, we employed a simple spin-coating process followed by electrochemical evaluation of a hydrogel-coated plate electrode. Initial attempts using a hydrogel composed of 3% (w/v) very high molecular weight chitosan and 1% (w/v) DAS were unsuccessful. This formulation resulted in a thick coating layer that hindered the escape of gas evolving on the electrode surface, ultimately leading to rupture of the coating. Consequently, no improvement in performance was observed (Fig. 12). In addition, the coating exhibited poor adhesion, resulting in detachment, delamination, and cracking, particularly in the central region of the plate electrode.

To achieve a thinner and more stable coating, a lower viscosity chitosan solution was required. Therefore, a 3% (w/v) low molecular weight chitosan solution was used, which demonstrated sufficient aerophobic behavior ($\alpha \geq 150°$) in the captive bubble contact angle test. This modification enabled successful coating formation, leading to enhanced aerophobicity and improved electrochemical performance of the electrode (Fig. 12). The results therefore demonstrate that the deposition of thin hydrogel layer is essential for enabling bubble passage through the hydrogel layer during bubble formation, and that even a low hydrogel loading on the electrode is effective for bubble repellency.

LSV measurements showed a notable performance increase, especially at higher overpotentials associated with hydrogen evolution. When comparing platinum hydrogel-coated electrodes with low MW chitosan, an increase in water-splitting efficiency was observed. Specifically, at a potential of −0.67 V, there is a clear increase in current density, from −0.17 A to −0.20 A, which corresponds to an approximately 15% enhancement. Despite the electrode being coated on only one side, a significant improvement was observed in the region of rapid hydrogen production. These results confirm the fundamental functionality of the coating. Overall, this straightforward evaluation demonstrates one of the potential applications of the developed chitosan/DAS hydrogels as superaerophobic coatings for electrodes in gas evolution processes.

4. Conclusion

In this study, we developed fully bio-based chitosan/DAS hydrogels with tunable aerophobic properties and good swelling stability in alkaline conditions. Influence of chitosan MW and concentration was systematically studied on their structure–property relationships were systematically evaluated. Increased concentrations (3-4% w/v) and MW of chitosan led to faster gelation, higher mechanical strength (up to

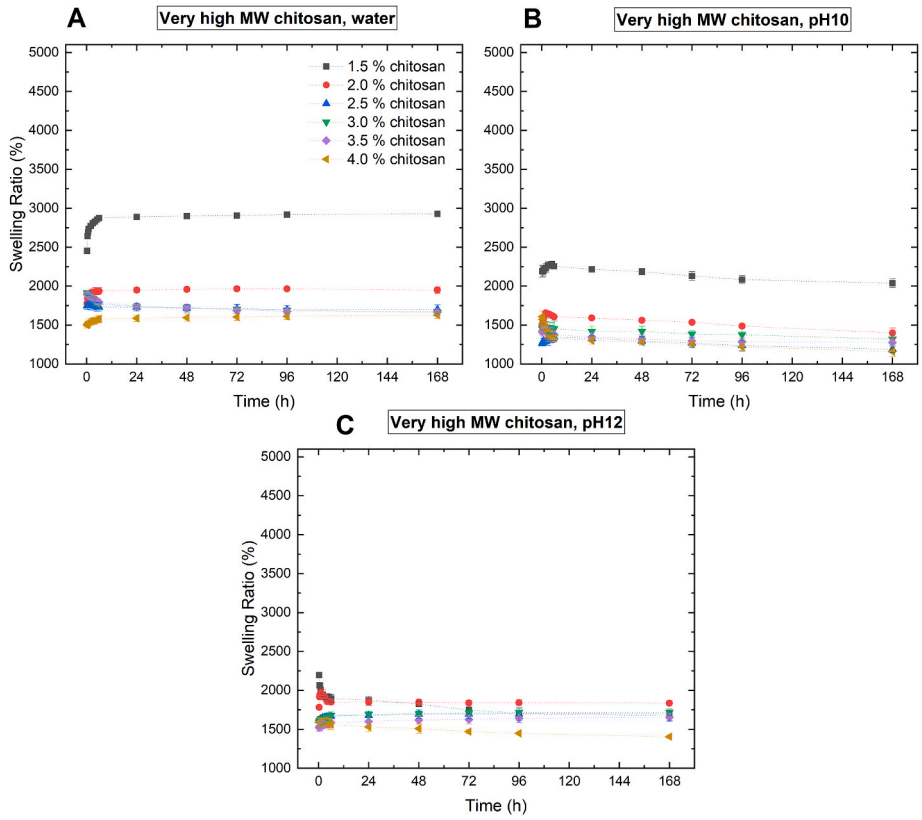


Fig. 10. Time-dependent swelling behavior of hydrogels with varying very high MW chitosan concentrations at constant DAS content under different pH conditions: (A) water, (B) pH 10, and (C) pH 12. Chitosan concentrations are: 1.5% (w/v) (gray), 2.0% (w/v) (red), 2.5% (w/v) (blue), 3.0% (w/v) (green), 3.5% (w/v) (purple), and 4.0% (w/v) (yellow). Data are means ± SD (n = 3). (For interpretation of the references to color in this figure legend, the reader is referred to the Web version of this article.)

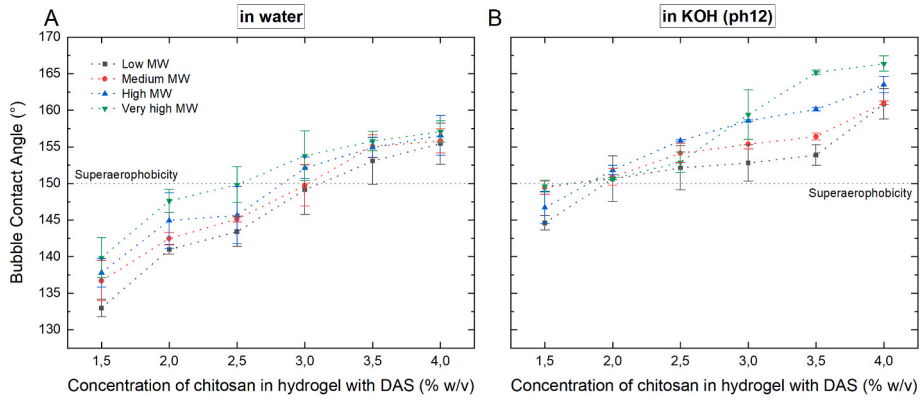


Fig. 11. Effect of chitosan concentration and MW on the aerophobic behavior of chitosan/DAS hydrogels in (A) water at pH 5.5 or (B) KOH solution at pH 12. MW is: low (gray), medium (red), high (blue), and very high (green) MW chitosan. Data are means ± SD (n = 3). (For interpretation of the references to color in this figure legend, the reader is referred to the Web version of this article.)

150 Pa of storage modulus after 30 min of gelation), while lower concentrations (1.5-2% w/v) resulted in weakly crosslinked networks with low storage modulus (down to 1 Pa after 30 min of gelation), high swelling ratios (up to ~5000%) and structural degradation. In contrast, higher concentration systems exhibited moderate swelling (1300-2000%) combined with long-term (7 days) stability, particularly under alkaline conditions. Aerophobicity was enhanced with increasing MW and polymer concentration, with air bubble contact angles reaching up to ~170°. This behavior was not solely dictated by hydrophilicity and is likely related to surface morphology and network integrity. SEM analysis confirmed that while pore size remained in the range of several tens of micrometers, polymer concentration significantly influenced pore interconnectivity and structural uniformity, with denser networks formed at higher concentrations. Increasing polymer concentration resulted in the formation of denser and mechanically stronger network structures. This was reflected in the physical, mechanical and surface properties, namely in reduced swelling, improved stability and maintained superaerophobicity.

The proof of concept was validated using a simple three-electrode system with LSV in 1 M KOH. Optimized coating thickness improves electrochemical performance by facilitating bubble detachment during gas evolution, especially at high overpotentials. In summary, this study

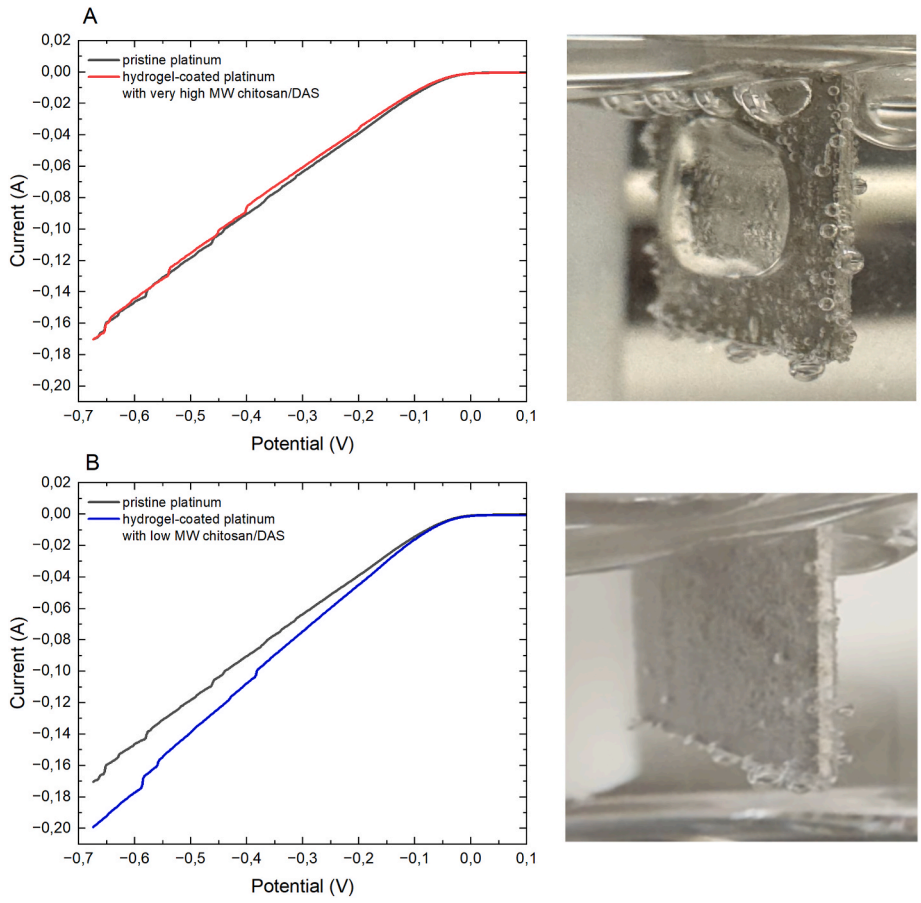


Fig. 12. LSV electrochemical performance of hydrogel-coated platinum electrodes using 3% (w/v) chitosan: (A) very high MW and (B) low MW, both crosslinked with 1% (w/v) DAS. The coated platinum electrodes (cathode) were tested in a three-electrode configuration with Hg/HgO reference and Pt/Ti mesh counter electrode. Measurements were performed at 25 °C and pH 14 in 1 M KOH electrolyte.

demonstrates that chitosan/DAS hydrogel is a tunable system, enabling control of its structural, mechanical and interfacial features via composition and network design. The alkaline-stable, porous and aerophobic nature of material makes it promising candidate for gas evolving electrochemical systems as a coating layer or a hydrogel electrolyte in water splitting device. Besides that, its favorable physiochemical features of completely bio-based material can also make it suitable for other applications such as energy storage devices, anticorrosion/antifouling coatings or sensing systems under harsh conditions.

CRediT authorship contribution statement

Vojtěch Škopek: Conceptualization, Data curation, Formal analysis, Investigation, Methodology, Project administration, Writing – original draft. **Ewa Olewnik-Kruszkowska:** Investigation, Methodology, Supervision, Writing – review & editing. **Magdalena Gierszewska:** Data curation, Methodology, Supervision, Writing – review & editing. **Iztok Dogsa:** Data curation, Methodology, Supervision, Writing – review & editing. **Paulius Pobedinskas:** Methodology, Resources. **Filipa A. Vicente:** Supervision. **Blaž Likozar:** Resources. **Ilja Gasan Osojnik Črnivec:** Project administration, Resources, Supervision, Writing – review & editing.

Acknowledgement

This work was financially supported by the Scientists4Future Slovenia project, the MSCA Seal of Excellence HORIZON-MSCA-2021-COFUND (2023-2027); P2-0152 Chemical Reaction Engineering programme (Slovenian Research and Innovation Agency, 2020-2027); DUBT Centre for Development, Demonstration and Training for Carbon-Free Technologies project (2023-2026); and CarbNETs TRL3-6 programme (2026-2029). *Scientists4Future Slovenia has received funding from Republic of Slovenia, Ministry of Higher Education, Science and Innovation. DUBT Centre is co-financed by the Republic of Slovenia, Ministry of Higher Education, Science and Innovation, and by the European Union under the Just Transition Fund. CarbNETS programme is co-funded by the Republic of Slovenia, Ministry of Education, Science and Youth, and by the European Union under the Cohesion Policy Fund.*

Appendix A. Supplementary data

Supplementary data to this article can be found online at https://doi.org/10.1016/j.biombioe.2026.109799.

Data availability

Data will be made available on request.

References

[1] T. Xu, K. Liu, N. Sheng, M. Zhang, W. Liu, H. Liu, L. Dai, X. Zhang, C. Si, H. Du, K. Zhang, Biopolymer-based hydrogel electrolytes for advanced energy storage/conversion devices: properties, applications, and perspectives, Energy Storage Mater. 48 (2022) 244–262, https://doi.org/10.1016/j.ensm.2022.03.013.

[2] Y. Guo, J. Bae, Z. Fang, P. Li, F. Zhao, G. Yu, Hydrogels and hydrogel-derived materials for energy and water sustainability, Chem. Rev. 120 (2020) 7642–7707, https://doi.org/10.1021/acs.chemrev.0c00345.

[3] S. Correa, A.K. Grosskopf, H. Lopez Hernandez, D. Chan, A.C. Yu, L.M. Stapleton, E. A. Appel, Translational applications of hydrogels, Chem. Rev. 121 (2021) 11385–11457, https://doi.org/10.1021/acs.chemrev.0c01177.

[4] X. Liu, J. Liu, S. Lin, X. Zhao, Hydrogel machines, Mater. Today 36 (2020) 102–124, https://doi.org/10.1016/j.mattod.2019.12.026.
[5] X. Zhao, Multi-scale multi-mechanism design of tough hydrogels: building dissipation into stretchy networks, Soft Matter 10 (2014) 672–687, https://doi.org/10.1039/c3sm52272e.
[6] X. Zhao, X. Chen, H. Yuk, S. Lin, X. Liu, G. Parada, Soft materials by design: unconventional polymer networks give extreme properties, Chem. Rev. 121 (2021) 4309–4372, https://doi.org/10.1021/acs.chemrev.0c01088.
[7] B. Jiang, Y. Long, X. Pu, W. Hu, Z.L. Wang, A stretchable, harsh condition-resistant and ambient-stable hydrogel and its applications in triboelectric nanogenerator, Nano Energy 86 (2021) 106086, https://doi.org/10.1016/j.nanoen.2021.106086.
[8] F. Mo, G. Liang, Q. Meng, Z. Liu, H. Li, J. Fan, C. Zhi, A flexible rechargeable aqueous zinc manganese-dioxide battery working at −20 °C, Energy Environ. Sci. 12 (2019) 706–715, https://doi.org/10.1039/C8EE02892C.
[9] Z. Wang, H. Li, Z. Tang, Z. Liu, Z. Ruan, L. Ma, Q. Yang, D. Wang, C. Zhi, Hydrogel electrolytes for flexible aqueous energy storage devices, Adv. Funct. Mater. 28 (2018) 1804560, https://doi.org/10.1002/adfm.201804560.
[10] S.C. Sutradhar, N. Banik, M.S. Ahmed, H. Jang, K.-W. Nam, M. Islam, Applications of hydrogels for next-generation batteries, Gels 11 (2025) 757, https://doi.org/10.3390/gels11090757.
[11] C. Wang, J. Li, Z. Zhou, Y. Pan, Z. Yu, Z. Pei, S. Zhao, L. Wei, Y. Chen, Rechargeable zinc-air batteries with neutral electrolytes: recent advances, challenges, and prospects, EnergyChem 3 (2021) 100055, https://doi.org/10.1016/j.enchem.2021.100055.
[12] Y. Wang, Q. Li, H. Hong, S. Yang, R. Zhang, X. Wang, X. Jin, B. Xiong, S. Bai, C. Zhi, Lean-water hydrogel electrolyte for zinc ion batteries, Nat. Commun. 14 (2023) 3890, https://doi.org/10.1038/s41467-023-39634-8.
[13] R. Wang, C. Xu, J.-M. Lee, High performance asymmetric supercapacitors: New NiOOH nanosheet/graphene hydrogels and pure graphene hydrogels, Nano Energy 19 (2016) 210–221, https://doi.org/10.1016/j.nanoen.2015.10.030.
[14] Y. Kang, S. Lee, S. Han, D. Jeon, M. Bae, Y. Choi, D.W. Lee, J. Ryu, Versatile, stable, and scalable gel-like aerophobic surface system (GLASS) for hydrogen production, Adv. Funct. Mater. 34 (2024), https://doi.org/10.1002/adfm.202308827.
[15] D. Jeon, J. Park, C. Shin, H. Kim, J.-W. Jang, D.W. Lee, J. Ryu, Superaerophobic hydrogels for enhanced electrochemical and photoelectrochemical hydrogen production, Sci. Adv. 6 (2020), https://doi.org/10.1126/sciadv.aaz3944 eaaz3944.
[16] H. Sarma, S. Mandal, A. Borbora, J. Das, S. Kumar, U. Manna, Self-healable, tolerant superaerophobic coating for improving electrochemical hydrogen production, Small 20 (2024) 2309359, https://doi.org/10.1002/smll.202309359.
[17] J. Das, E. Özdemir, H. Sarma, A. Terfort, U. Manna, Hydrogen-bubble repellent conjugated polymeric coating for improving electrochemical hydrogen evolution, Adv. Funct. Mater. 35 (2025) 2505403, https://doi.org/10.1002/adfm.202505403.
[18] M. Bae, Y. Kang, D.W. Lee, D. Jeon, J. Ryu, Superaerophobic polyethyleneimine hydrogels for improving electrochemical hydrogen production by promoting bubble detachment, Adv. Energy Mater. 12 (2022) 2201452, https://doi.org/10.1002/aenm.202201452.
[19] J. Ding, Y. Yang, J. Poisson, Y. He, H. Zhang, Y. Zhang, Y. Bao, S. Chen, Y.M. Chen, K. Zhang, Recent advances in biopolymer-based hydrogel electrolytes for flexible supercapacitors, ACS Energy Lett. 9 (2024) 1803–1825, https://doi.org/10.1021/acsenergylett.3c02567.
[20] Y. Wang, X. Zhang, X. Zhao, X. Yang, M. Yuan, Y. Zheng, J. Tang, W. Liu, J. Zhang, L. Lin, Excellent electrochemical performance based on covalently crosslinked chitosan hydrogel electrolytes induced structural stability against alkali, Adv. Compos. Hybrid Mater. 8 (2025) 183, https://doi.org/10.1007/s42114-024-01191-z.
[21] C. Li, S. Yang, Y. Guo, H. Lv, P. Li, X. Bai, X. Li, C. Zhi, H. Li, Hydrogel electrolyte with high tolerance to a wide spectrum of pHs and compressive energy storage devices based on it, Small Methods 7 (2023) 2201448, https://doi.org/10.1002/smtd.202201448.
[22] L. Huang, X. Han, Q. Mo, Y. Wang, X. Wang, Y. Li, C. Huang, Q. Duan, Preparation and properties of modified cassava starch slow-release hydrogel with acid and alkali resistance, Ind. Crops Prod. 206 (2023) 117699, https://doi.org/10.1016/j.indcrop.2023.117699.
[23] E. Cohen, E. Poverenov, Hydrophilic chitosan derivatives: synthesis and applications, Chem. Weinh. Bergstr. Ger. 28 (2022) e202202156, https://doi.org/10.1002/chem.202202156.
[24] P. Wang, Y. Wang, P. Hong, C. Zhou, Di-aldehyde starch crystal: a novel bio-crosslinker for strengthening the structure and physio-chemical properties of gelatin-based films, Food Biosci. 43 (2021) 101308, https://doi.org/10.1016/j.fbio.2021.101308.
[25] Y. Zuo, W. Liu, J. Xiao, X. Zhao, Y. Zhu, Y. Wu, Preparation and characterization of dialdehyde starch by one-step acid hydrolysis and oxidation, Int. J. Biol. Macromol. 103 (2017) 1257–1264, https://doi.org/10.1016/j.ijbiomac.2017.05.188.
[26] Y. Liu, H. Zhao, Y. Fang, Z. Wu, B. Yu, B. Cui, Hydrogels of dialdehyde starch and gelatin cross-linked with potential application as tissue adhesives, Int. J. Biol. Macromol. 289 (2025) 138956, https://doi.org/10.1016/j.ijbiomac.2024.138956.
[27] S. Aslzad, P. Savadi, E.D. Abdolahinia, Y. Omidi, M. Fathi, J. Barar, Chitosan/dialdehyde starch hybrid in situ forming hydrogel for ocular delivery of betamethasone, Mater. Today Commun. 33 (2022) 104873, https://doi.org/10.1016/j.mtcomm.2022.104873.
[28] S. Grabska-Zielińska, A. Sionkowska, K. Reczyńska, E. Pamuła, Physico-chemical characterization and biological tests of collagen/silk fibroin/chitosan scaffolds cross-linked by dialdehyde starch, Polymers 12 (2020) 372, https://doi.org/10.3390/polym12020372.
[29] E.A. Kamoun, N-succinyl chitosan–dialdehyde starch hybrid hydrogels for biomedical applications, J. Adv. Res. 7 (2016) 69–77, https://doi.org/10.1016/j.jare.2015.02.002.
[30] X. Yu, Z.-Y. Yu, X.-L. Zhang, Y.-R. Zheng, Y. Duan, Q. Gao, R. Wu, B. Sun, M.-R. Gao, G. Wang, S.-H. Yu, "Superaerophobic" nickel phosphide nanoarray catalyst for efficient hydrogen evolution at ultrahigh current densities, J. Am. Chem. Soc. 141 (2019) 7537–7543, https://doi.org/10.1021/jacs.9b02527.
[31] Y. Kang, S. Lee, J. Lee, S. Lee, G. Lee, H. Kim, G.H. Choi, J. Ryu, D.W. Lee, Anisotropically wettable porous transport layers for gas management in water electrolyzers, Adv. Sci. 13 (2026) e08569, https://doi.org/10.1002/advs.202508569.
[32] S. Bashir, M. Hina, J. Iqbal, A.H. Rajpar, M.A. Mujtaba, N.A. Alghamdi, S. Wageh, K. Ramesh, S. Ramesh, Fundamental concepts of hydrogels: synthesis, properties, and their applications, Polymers 12 (2020) 2702, https://doi.org/10.3390/polym12112702.
[33] D.N. Ampong, E. Agyekum, P. Dzikunu, D. Ocloo, I. Clottey, P. Aggrey, M. A. Nartey, F.O. Agyemang, K. Mensah-Darkwa, R.K. Gupta, Harnessing hydrogels for electrochemical energy and environmental sustainability, Renew. Sustain. Energy Rev. 229 (2026) 116628, https://doi.org/10.1016/j.rser.2025.116628.
[34] J. Wen, J. Lei, J. Chen, J. Gou, Y. Li, L. Li, An intelligent coating based on pH-sensitive hybrid hydrogel for corrosion protection of mild steel, Chem. Eng. J. 392 (2020) 123742, https://doi.org/10.1016/j.cej.2019.123742.
[35] D. Liu, H. Shu, J. Zhou, X. Bai, P. Cao, Research progress on new environmentally friendly antifouling coatings in marine settings: a review, Biomimetics 8 (2023) 200, https://doi.org/10.3390/biomimetics8020200.
[36] L. Chen, Y. Ding, J. Gong, H. Xie, J. Qu, R. Niu, Molecular engineering of biomass-derived hybrid hydrogels for solar water purification, J. Colloid Interface Sci. 626 (2022) 231–240, https://doi.org/10.1016/j.jcis.2022.06.145.
[37] S. Lee, J. Lee, S. Lee, H. Kim, Y. Kang, D.W. Lee, J. Ryu, Superaerophobic hydrogels for diaphragm modification to suppress gas crossover in alkaline water electrolyzers, J. Mater. Chem. A (2026), https://doi.org/10.1039/D5TA07926H.
[38] S. Zong, H. Lv, C. Liu, L. Zhu, J. Duan, J. Jiang, Mussel inspired Cu-tannic autocatalytic strategy for rapid self-polymerization of conductive and adhesive hydrogel sensors with extreme environmental tolerance, Chem. Eng. J. 465 (2023) 142831, https://doi.org/10.1016/j.cej.2023.142831.
[39] L.-Y. Zhang, D.-Q. Feng, P.-Y. Zhu, W.-L. Song, M. Yasir, C. Zhang, L. Liu, Hydrogel-anchored Fe-Based amorphous coatings with integrated antifouling and anticorrosion functionality, ACS Appl. Mater. Interfaces 15 (2023) 13644–13655, https://doi.org/10.1021/acsami.3c00227.
[40] W. Luo, Y. Zuo, Y. Zheng, X. Long, F. Jiao, Double network cross-linked hydrogel coating membrane with photocatalytic self-cleaning performance for efficient oil-water separation, Prog. Org. Coat. 185 (2023) 107882, https://doi.org/10.1016/j.porgcoat.2023.107882.
[41] J. Das, S. Mandal, A. Borbora, S. Rani, M. Tenjimbayashi, U. Manna, Modulating force of nucleated hydrogen bubble adhesion to boost electrochemical water splitting, Adv. Funct. Mater. 34 (2024) 2311648, https://doi.org/10.1002/adfm.202311648.
[42] J. Park, D. Jeon, Y. Kang, J. Ryu, D.W. Lee, Nanofibrillar hydrogels outperform Pt/C for hydrogen evolution reactions under high-current conditions, J. Mater. Chem. A 11 (2023) 1658–1665, https://doi.org/10.1039/D2TA08775H.
[43] X. Huang, L. Zhang, Encapsulation of hydrogel sensors, Chem. Eng. J. 484 (2024) 149631, https://doi.org/10.1016/j.cej.2024.149631.
[44] T.K.L. Nguyen, T.-N. Pham-Truong, Recent advancements in gel polymer electrolytes for flexible energy storage applications, Polymers 16 (2024) 2506, https://doi.org/10.3390/polym16172506.
[45] C. Li, S. Yang, Y. Guo, H. Lv, P. Li, X. Bai, X. Li, C. Zhi, H. Li, Hydrogel electrolyte with high tolerance to a wide spectrum of pHs and compressive energy storage devices based on it, Small Methods 7 (2023) e2201448, https://doi.org/10.1002/smtd.202201448.
[46] R.A.A. Muzzarelli, R. Rocchetti, The determination of the degree of acetylation of chitosans by spectrophotometry, in: R. Muzzarelli, C. Jeuniaux, G.W. Gooday (Eds.), Chitin Nat. Technol., Springer, US, Boston, MA, 1986, pp. 385–388, https://doi.org/10.1007/978-1-4613-2167-5_47.
[47] M. Ziegler-Borowska, K. Wegrzynowska-Drzymalska, D. Chelminiak-Dudkiewicz, J. Kowalonek, H. Kaczmarek, Photochemical reactions in Dialdehyde Starch, Molecules 23 (2018) 3358, https://doi.org/10.3390/molecules23123358.
[48] M.R. Kasaai, A review of several reported procedures to determine the degree of *N*-acetylation for chitin and chitosan using infrared spectroscopy, Carbohydr. Polym. 71 (2008) 497–508, https://doi.org/10.1016/j.carbpol.2007.07.009.
[49] T.A. Khan, K.K. Peh, H.S. Ch'ng, Reporting degree of deacetylation values of chitosan: the influence of analytical methods, J. Pharm. Pharm. Sci. Publ. Can. Soc. Pharm. Sci. Soc. Can. Sci. Pharm. 5 (2002) 205–212.
[50] M.L. Duarte, M.C. Ferreira, M.R. Marvão, J. Rocha, An optimised method to determine the degree of acetylation of chitin and chitosan by FTIR spectroscopy, Int. J. Biol. Macromol. 31 (2002) 1–8, https://doi.org/10.1016/s0141-8130(02)00039-9.
[51] A. Domard, M. Rinaudo, Preparation and characterization of fully deacetylated chitosan, Int. J. Biol. Macromol. 5 (1983) 49–52, https://doi.org/10.1016/0141-8130(83)90078-8.
[52] R. Czechowska-Biskup, D. Jarosińska, B. Rokita, P. Ulański, J. Rosiak, Determination of degree of deacetylation of chitosan - Comparision of methods, Prog. Chem. Appl. Chitin Its Deriv. 2012 (2012) 5–20.
[53] J. Brugnerotto, J. Lizardi, F.M. Goycoolea, W. Argüelles-Monal, J. Desbrières, M. Rinaudo, An infrared investigation in relation with chitin and chitosan characterization, Polymer 42 (2001) 3569–3580, https://doi.org/10.1016/S0032-3861(00)00713-8.